Commissioning of the WWFI for the Wendelstein Fraunhofer Telescope

Claus Gössl[a], Ralf Bender[a,b], Maximilian Fabricius[a], Ulrich Hopp[a,b], Adolf Karasz[a], Ralf Kosyra[a], Florian Lang-Bardl[a]

[a]Universitäts-Sternwarte München, Scheinerstr. 1, D81579 München, Germany;
[b]Max Planck Institut für Extraterrestrische Physik, Gießenbachstrasse, D85748 Garching, Germany

ABSTRACT

Ludwig-Maximilians-Universität München operates an astrophysical observatory on the summit of Mt. Wendelstein[1] which has been equipped with a modern 2m-class telescope.[2–4] The new *Fraunhofer* telescope is designed to sustain the excellent (< 0.8" median) seeing of the site [1, Fig. 1] over a FoV of 0.2 deg^2 utilizing a camera built around a customized 64 MPixel Mosaic (Spectral Instruments, $4 \times (4k)^2$ 15μm e2v CCDs). The **W**endelstein **W**ide **F**ield **I**mager[5] had its commissioning in the lab in the course of the last few months and now waits to see first light on sky in the near future, i.e. when telescope commissioning allows to test science instruments.

Keywords: CCD camera, wide field

1. INTRODUCTION

It is a challenging task to build a complete suite of instruments (two new imagers, WWFI[5] and 3kk;[6] a field spectrograph VIRUSW,[7,8] and an upgraded high resolution Echelle spectrograph FOCES;[9–11] the latter three mounted on / fed through a common port[12]) while supporting the building and installation of the new telescope[2–4] and its observatory infrastructure with a team of about six within four years. This could only be achieved by relying on existing solutions wherever possible. We bought CCD detector systems from a broad range of companies, since it turned out there was no single system (or even company) which could satisfy the different needs (and budgets) of all instrumentation projects. Bonn Shutters are employed for the WWFI, 3kk and VIRUSW. For the NIR part of 3kk we relied on the expertise of our partner (IfA at Hilo, Hawaii). With VIRUSW already gathering science data (being on loan at McDonald observatory),[8] and the FOCES[10,11] upgrades continuing in the lab we have postponed the completion of 3kk in favor of getting the WWFI ready for first light as soon as possible, as the WWFI is also the only instrument which can verify telescope perfomance including the wide field corrector. Our efforts greatly benefit from the work and enthusiasm of highly motivated students who have the chance to collect real hands-on expertise within our instrumentation projects.

At the last SPIE Astronomical Telescopes and Instrumentation conference in 2010 we presented the overall camera layout and design as well as the projected performance of the WWFI:[5] The imager will map a FoV of 0.7 degree in diameter utilizing three-element transmissive field corrector optics for optical wavebands. The last lens of this corrector serves as entrance lens of the dewar of the WWFI Mosaic CCD system. To fully profit from the typically outstanding seeing quality of the site,[1,4] a sampling of 0.2 arcsec per pixel is required. FoV and sampling ask for a large CCD detector of $\sim$ 16k$\times$16k which is realized by a 2×2 mosaic of 4k e2v chips. To secure the image quality, high structural stability and off-axis guiding was mandatory. We developed a compact, triple-stage and partially Serrurier design, aligning the off-axis guider unit, a Bonn shutter, two filter wheels, and the detector system in a row. Two guider systems, each equipped with a 2k Fairchild CCD, control guiding and derotator behavior of the alt-az mounted telescope. A highly reliable EMI* safety of the instrument envelope is enforced by the nearby powerful radio antenna. Here, we will report on detector system verification and camera assembly with some details on the "not-straight-foward" topics we have encountered.

Further author information: (Send correspondence to C.G.)
C.G.: E-mail: cag@usm.uni-muenchen.de, Telephone: +49 89 2180 5972
*electromagnetic interference

Ground-based and Airborne Instrumentation for Astronomy IV, edited by Ian S. McLean, Suzanne K. Ramsay, Hideki Takami, Proc. of SPIE Vol. 8446, 84463P · © 2012 SPIE · CCC code: 0277-786X/12/$18 · doi: 10.1117/12.926341

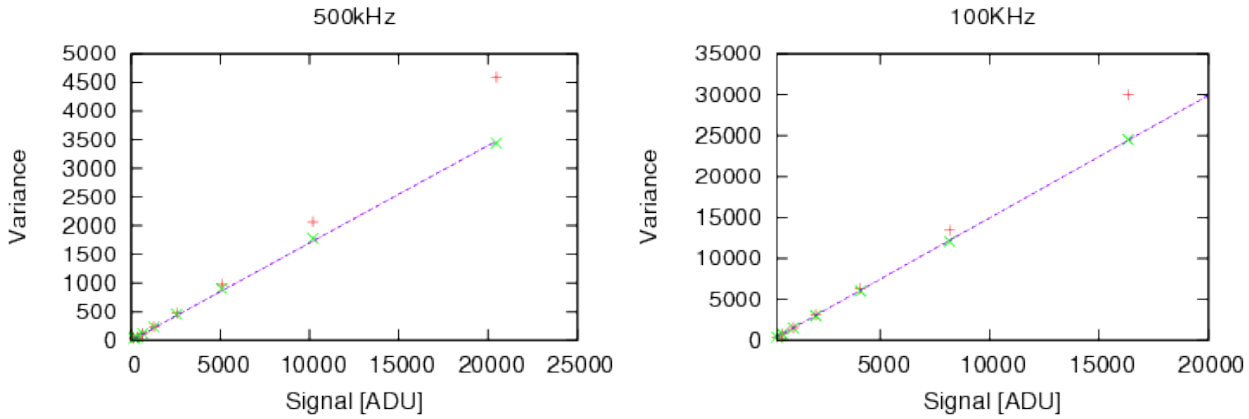

Figure 1. Photon transfer for the 500KHz readout mode (left) and the 100KHz mode (right), with the signal in ADU on the x-axis and the variance on the y-axis. (Example of one port of one CCD.) The red "+" show the uncorrected values while the green "x" show the variances corrected for the noise of the masterflat.

2. DETECTOR SYSTEM VERIFICATION

2.1 Basic Parameters

We expanded our test bench for the filter tests (double monochromator / photodiode) with an Ulbricht sphere to verify the basic parameters of all the CCD systems we have purchased.

2.1.1 Gain

The "gain" of a photon collecting device is given by the ratio $g = e^-/\text{ADU}$ (electrons per Analog Digital Units). To measure the gain factor we made use of the "photon transfer gain method": We make a series of homogeneously illuminated images with different exposure times. All images get the bias subtracted and are divided by a "masterflat" (composed of 30 single flatfield images significantly below half of full-well) for removing the pixel noise[†] from the images. Then we determine the mean signal and variance of every image. For further considerations we can neglect the readout noise (RoN) as it is well below the photon noise, so the photon noise σ is the only source of variance σ^2 left in an image with an average signal S. We get

$$\sigma^2 = \frac{S}{g}. \tag{1}$$

Unfortunately, the introduction of the masterflat M adds another source of noise: The red "+" in Fig. 1 (indicating F_i and $\sigma^2_{F_i}$) show that the data points at high signal levels deviate from linear behavior which one would expect from a simple, undisturbed signal (S_i and $\sigma^2_{S_i}$) because of the residual photon noise in the masterflat σ_M. Since the arithmetic operation that creates our final signal files is a division, the relative noises add in quadrature:

$$\left(\frac{\sigma_{F_i}}{F_i}\right)^2 = \left(\frac{\sigma_M}{M}\right)^2 + \left(\frac{\sigma_{S_i}}{S_i}\right)^2 \tag{2}$$

with S_i the average signal in the original exposure (index i for number of the exposure), M the average signal of the masterflat and F_i the average signal in the final image (divided by the masterflat) and the σ the

[†]The noise due to systematic small scale variability in an image, i.e. the "stable" non-uniformity of the pixels.

Table 1. Average Gain and Readout noise measured by ourselves (USM) and the manufacturer (SI).

Readout mode	Gain [e^-/ ADU]		Noise [e^-]	
	USM	SI	USM	SI
500 kHz	5.88	5.89	7.0	8.1
100 kHz	0.67	0.72	2.1	2.4

corresponding photon noises. With Eqn. 1 and the assumption $S_i = F_i$ (as the masterflat is normalized $M = 1$) one can calculate the gain from equation 2:

$$g = \frac{\frac{1}{F_i} - \frac{1}{F_j}}{\left(\frac{\sigma_{F_i}}{F_i}\right)^2 - \left(\frac{\sigma_{F_j}}{F_j}\right)^2} \tag{3}$$

for any indices $i \neq j$. The estimation of the gain with Eqn. 3 allows the determination of the (relative) photon noise in the masterflat, again via Eq. 1, which can be subtracted in Eq. 2 to obtain the true pure photon noise of the individual images, i.e. without the contribution of the masterflat. Fig. 1 shows the photon transfer functions for the 500 kHz (left) and 100 kHz (right) readout mode, with red "+" for uncorrected values and green "x" for values corrected for the noise of the masterflat. Finally, the gain has been determined by a linear fit to the corrected values (Tab. 1).

2.1.2 Readout noise

The readout noise has been measured from a sample of bias images by determination of the noise of a 1000×1000 pixel sample and clipping of outliers above sigma of 3. Tab. 1 shows the readout noise for both modes measured in our lab compared to the results of the manufacturer. The systematically lower values in our measurements can be explained by the different method: the manufacturer measured the noise from a subtracted image of two bias images, in which the noise is supposed to be higher by a factor of $\sqrt{2}$. The fact that the difference of the results of the two methods is less than the expected factor of $\sqrt{2}$ is because clipping does not account for additional systematic noise which can be overcome with a master bias subtraction.

2.2 Charge Persistence

Optical tests performed with the CCDs of the WWFI in the laboratory indicated a persistence of charges on the chip in regions where the detector had been saturated. The time constant of the persistent charges is in the order of ~ 10 min, which can be critical for many astronomical observations.

Several tests have been performed with the aim to determine how the time constant of the persistent charges depends on different quantities. These quantities are:

- The temperature of the chip
- The intensity of the incident light
- The wavelength of the incident light

Charge persistence is assumed to be caused by electron traps that come from lattice defects on the detector. When the charge in one pixel exceeds the full well capacity, the exceeding charges can be captured by the traps and diffuse out of them over time.

Table 2. Decade decay times for different chip temperatures as obtained with exponential fitting.

T [° C]	-115	-105	-95	-90	-88	-86	-84	-82	-80
Time constant [s per decade]	611	586	539	546	535	482	473	480	485

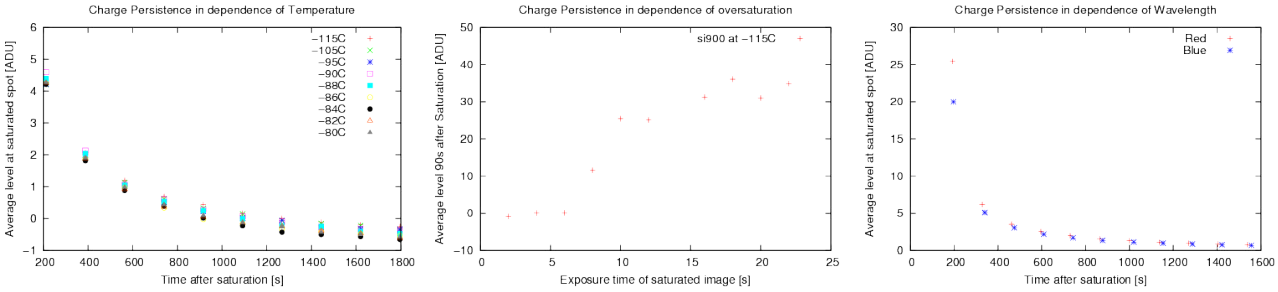

Figure 2. Left: Average charge as a function of time (after saturation) for different chip temperatures. Middle: Average charge [ADU] 90s after an exposure vs. exposure time used to cause saturation. Right: Charge per pixel as a function of time (after saturation) for red and blue light.

2.2.1 Temperature dependence

It is assumed that the average escape time of a trapped electron depends on its thermal energy and thus, the time constant of the persistent charges is probably of function of chip temperature. Measurements have been performed to investigate this dependence by oversaturating the detector in a defined region and analyzing the residual charges in a 100×100 pixel region in defined time intervals after the exposure.

Fig. 2 left shows the average charge in the 100×100 pixel region as a function of time, where the time zero-point is the moment when the detector is saturated. Tab. 2 shows the time constants (per decade) obtained by fitting an exponential function to the data sets. The decay times are dropping by a factor of $\sim$0.8 at -80° C compared to -115° C, but since the statistical error in this measurement is $\sim$ 50 s, it is mathematically not possible to describe the dependence between decay time and temperature with these data.

2.2.2 Intensity dependence

No persistent charges have been observed below saturation level. One may conclude that the behavior of the charge decay could depend on the amount of incident light above saturation level: A series of exposures with varying exposure times has been taken, to check this assumption. The varying exposure times cause different levels of oversaturation. Fig. 2 middle shows the average charge (in ADUs) in the oversaturated region 90s after the exposure vs. the exposure time of the initial image (which is a measure for the light level in oversaturated image). At the first three data points (up to 6s exposure time) the light level was below saturation and no persistent charge was detected. For exposure times above 6s the signal after 90s rises to a maximum value which is reached at about 10s exposure time. With longer exposure times the amount of persistent charges does not rise further, which means that there is only a narrow region in intensity, starting slightly above saturation, at which the amount of persistent charges depends on the light level. Below that region there is no charge persistence, and above that region charge persistence not not a function of light level anymore.

2.2.3 Wavelength dependence

For red light, the penetration depth is higher in the CCD chip than for blue light, which is absorbed closer to the surface. Since we do not know whether the electron traps are distributed uniformly over the whole volume of the chip, it is possible that either blue or red light causes a larger amount of charge persistence, depending on the density of traps at the surface or deeper within the bulk.

The right panel of Fig. 2 shows the amount of persistent charge as function of time after saturation for red and blue light. The graph clearly shows that there is no difference in the behavior of the charge decay depending on the wavelength of of the incident light.

3. CAMERA ASSEMBLY

3.1 Mechanical Integration

The modular concept of the WWFI has been detailed in the 2010 SPIE proceedings [5, see Sec. 4 and Fig. 3]. Mechanical integration of WWFI was done at USM in 2011 utilizing a test flange which has an identical interface as the Fraunhofer telescope Nasmyth ports (see Fig. 3). We successively built up the camera testing assembling before the black anodizing of most parts took place. The test assembly in the lab with ample space was also necessary to help us to decide how far we have to disassemble the camera for transport and how to reassemble it again at the telescope with only limited space availabe to work.

A flexure test of the main truss (see Fig. 3 top right) has indicated an maximum absolute displacement at image plane of $\approx 0.02\,\mathrm{mm}$ which is more than a factor of three below what finite elements analysis had predicted [5, see Sec. 4].

3.2 EMI Protection

The fabrication of the EMI proof cover (see Fig. 4) posed unforeseen problems as we found no company which would assemble the housing within the margin of error from design, so, we had to do it ourselves. The original design relied on conductively glueing the chromated aluminium metal sheets and truss together. Unfortunately, high conductive glues have about 80% filling of silver (or a similar conductive metal) and are much less adhesive than "normal" glues. Therefore, we partially changed the design to allow for all sheets to be screwed onto the minimal truss in addition. So now, the glue only has to provide the EMI seal while the screws keep the parts together.

3.3 Supply and Control Lines

Most modern scientific instruments house a great multitude of supply and control lines and interfaces. This is even more true for an instrument like the WWFI which is built around partially complex but nevertheless off-the-shelf components (see Fig. 5 and 6). As EMI considerations are essential external interfaces are kept to a minimum, i.e. the WWFI has feedthroughs for cooling water, PT30 cryo lines, fiber optical links, and 220 VAC, the latter employing interference filters[‡]. Internally there are many distributed but interconnected components which have only very few cabling paths "in common". We build a cable harness where appropriate but allow cabling "shortcuts" to keep "single" lines short and easy to access. Thermal switches are built into the power supply circuits of the controller and detector compartment of the camera and the cryo compressor cabinet as safeguards for cooling water failure.

During tests one of the FLI guiding cameras had a cooling water leak. Despite flow control one of the four internal plastic hose clips were insufficient to fix the tube to its connector. Since the leak caused a costly repair we decided to improve the system with better seals and longer connectors which allow for "real" hose clamps. And, we removed the tube "interface" of the cameras: Less connectors are less points of failure. Additional thermal switches with sensors glued on the backplate of the internal heat exchangers provide safety in case of cooling water failure.

We plan to off-load the two Mini-PCs which run the SI900 (Windows) and FLI (Linux) software to a remote cabinet as soon as basic operation on-site has been verified (see dashed lines in Fig. 5) to further reduce the heat load on the instrument and allow for an easier physical access to the PCs for maintenance. The SI900 fiber optical link deploys no Ethernet interface and therefore has to be patched through separately and cannot be switched. The FLI cameras are driven through USB 2.0 interfaces and will be connected to a USB-to-Ethernet converter (and vice versa) which allows to use the existing Ethernet fiber optical link.

[‡]The cryo compressors get their power through relays in the camera. Therefore, two interference filters have to work in a not so common way, protecting the power "source" and not the consumer.

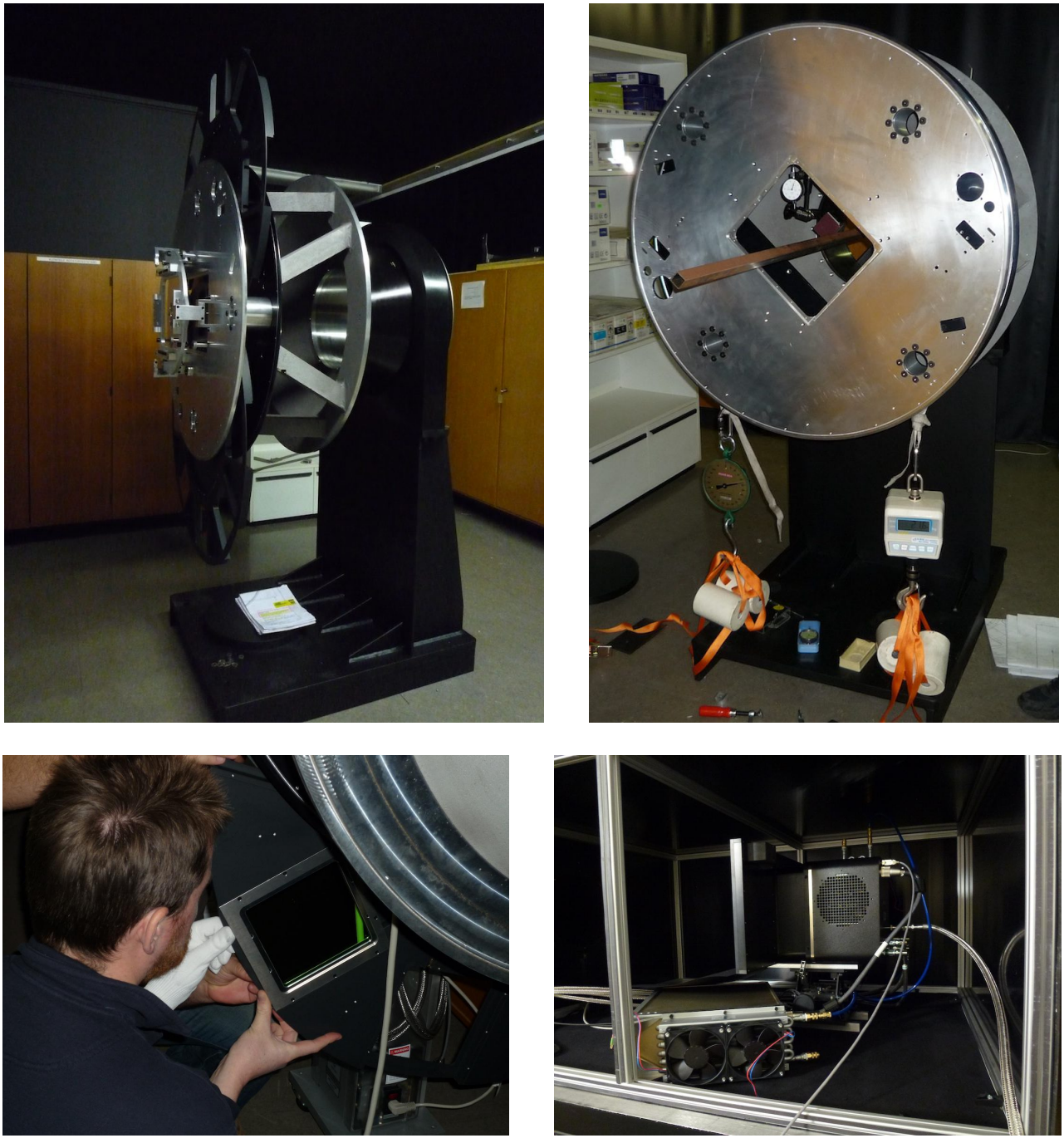

Figure 3. Pictures of WWFI integration. Top left: Main WWFI truss with filter wheels and tip-/tilt stage for the SI900. Top right: Flexure test of the truss shows that flexure is well within specs. Bottom left: Test insertion of filter within its cartridge. Bottom right: SI900 within our optical test bench. Proof of concept for the heat exchangers of the controller and detector compartment (CDC).

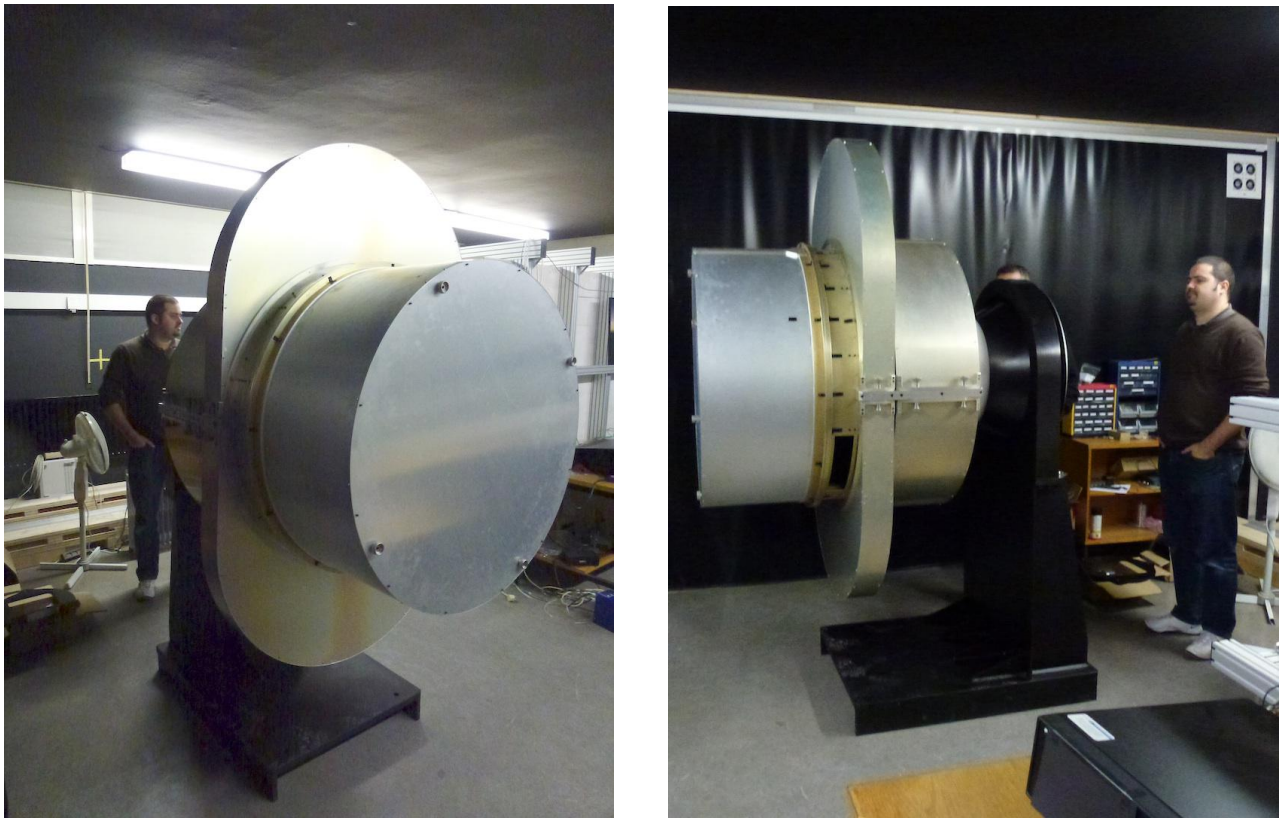

Figure 4. WWFI EMI proof cover: WWFI mounted on test flange in USM lab. All chromated covers attached.

4. SOFTWARE

Low level interface programs to communicate with the camera subcomponents in a simple, standardized, and human readable way have been developed and passed the stage of lab testing. The programs are written in C++ and rely on object oriented programming to keep the code base small and manageable. All programs connect to the subcomponents either directly via TCP/IP or using a serial-to-ethernet converter or, in case of the FLI cameras, by utilizing the FLI SDK to talk to the USB cameras: The SI900 is controlled by a Windows software which has an TCP/IP socket interface to allow for external control. The Bonn shutter, while being directly triggered through the SI900, is monitored through its serial interface and a dedicated interface program. We use Pollux Drive Controllers through their serial interface for the guider offset focus drives and the filter wheel drives. For the focus drives the software is rather simple as the controllers are set up to allow basic commands utilizing a motor and two limit switches. It turned out to be quite tricky to employ the same controllers for the filter wheels which have no "upper" and "lower" limit but a reference and a "on-position" switch instead[§].

Motors are powered off while the filter wheel is not moving and is on position secured by lock notches. The interface program for the FLI USB guiding cameras runs on a Mini-PC with a Tiny Core Linux.

5. STATUS – PROJECT TIMELINE

Test assembly of the camera has been completed. All components of the camera have been evaluated and tested in the lab. The lower level camera software routines are completed while mid- and high level software (i.e. integration within the observatory environment) will be developed during the one-year commissioning phase of the telescope. The camera is ready to be shipped to the observatory in June/July 2012 and will be installed at the telescope as soon as telescope commissioning allows.

[§]The interface software has to deactivate the limit switches to allow to leave a position but has to reactivate the limit switches in a timely manor during movement.

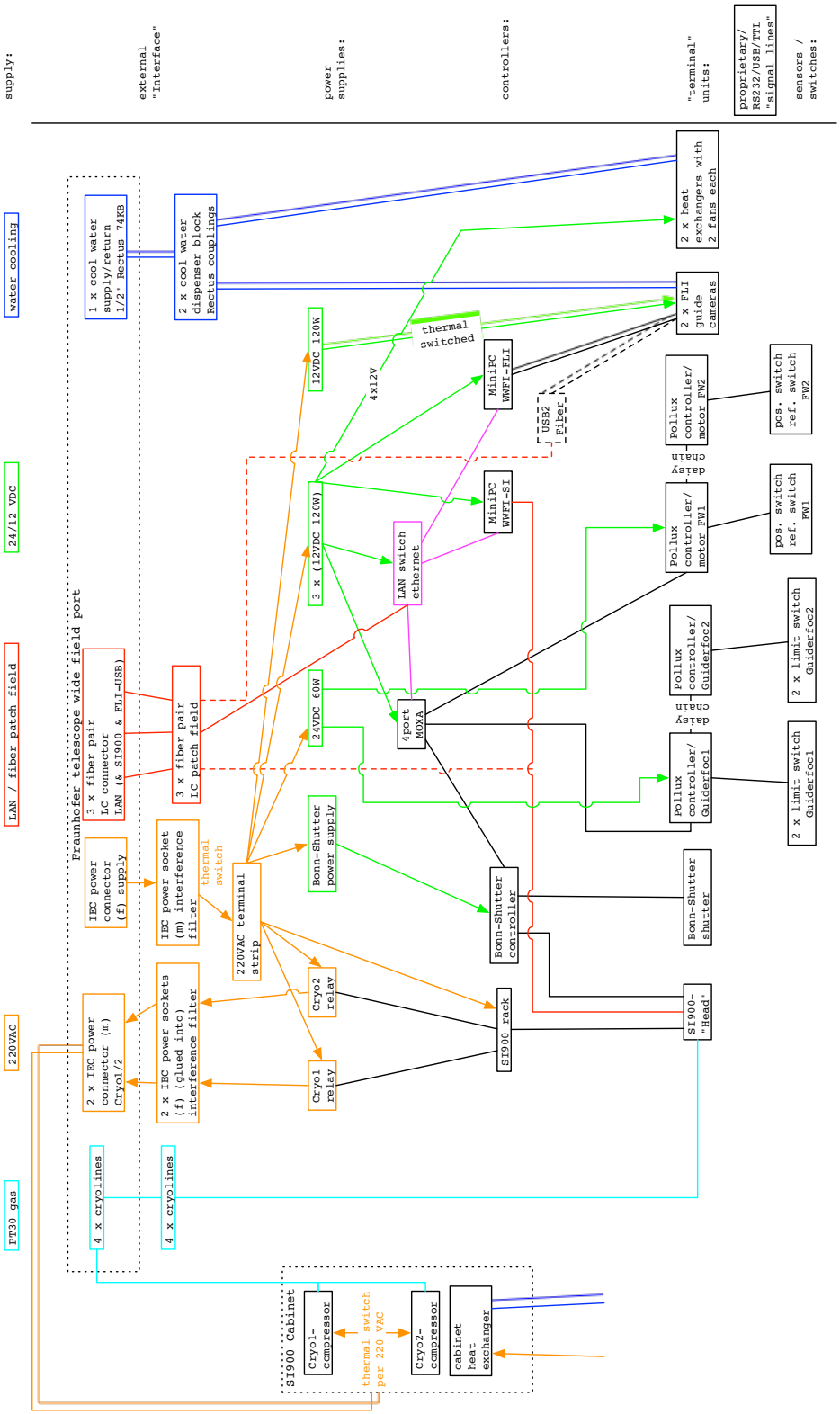

Figure 5. WWFI lines sketch: orange = 220VAC power lines, green = 24 or 12 VDC power lines, blue = cooling water lines, cyan = PT30 cryo lines, red = optical fiber data/control lines, magenta = LAN ethernet lines, black = control/drive lines i.e. RS232, USB, TTL or proprietary signal lines. Dashed: alternate lines when off-loading the Mini-PCs.

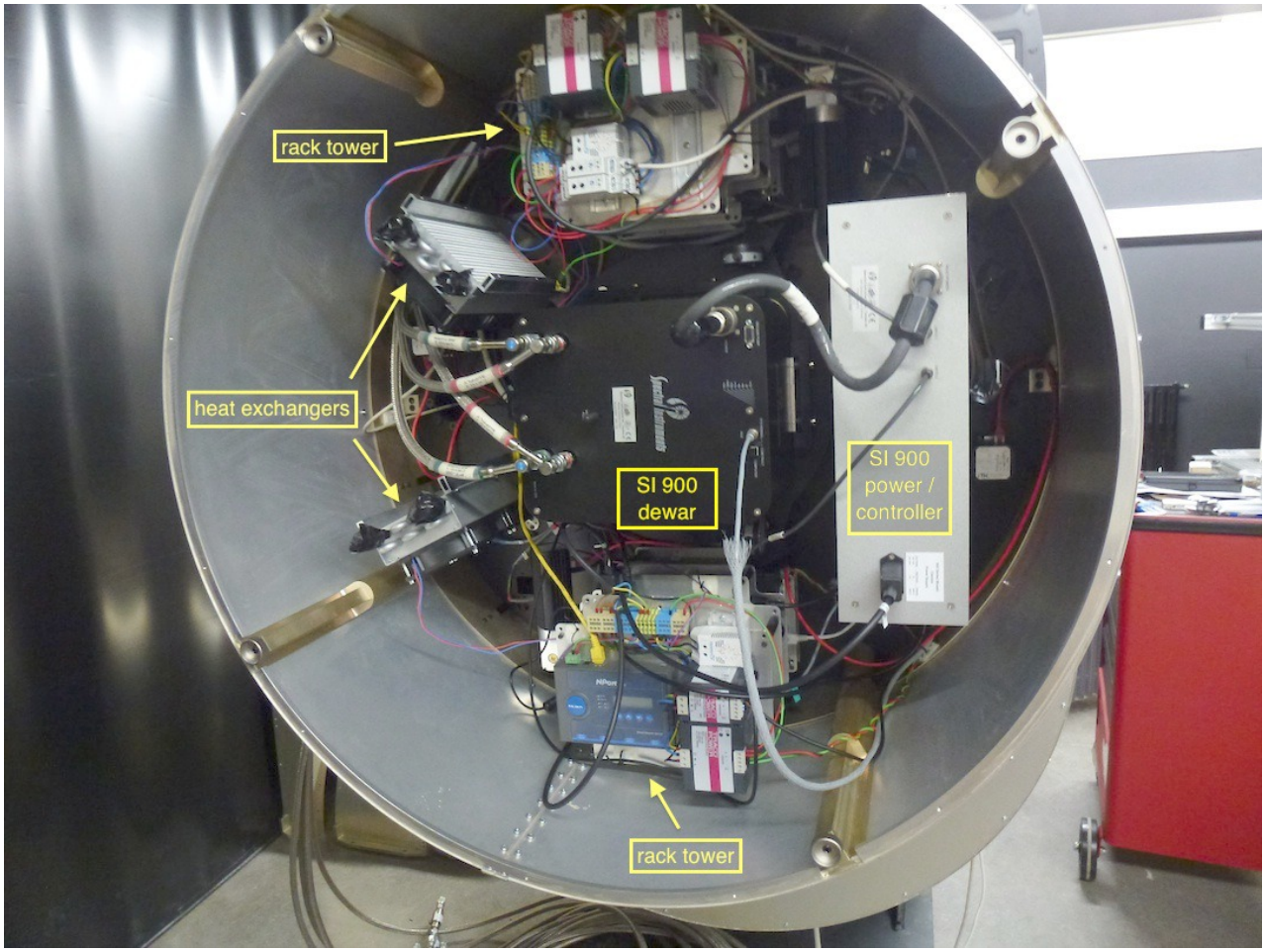

Figure 6. WWFI controller and detector compartment (CDC) during provisional cabling for testing, final metal sheet of the EMI safety enclosure still not glued in. The black detector dewar (center) is mounted in its tip-/tilt stage. The SI 900 controller/power supply on the right side is close to the mosaic dewar to allow for a short cable (EMI). The two (silver) heat exchangers with blowers in combination with the blowers of the SI900 dewar and controller will produce a "clockwise" circulation in the CDC. Top and bottom are two racks which hold most of the smaller devices, e.g. MiniPCs, DC power supplies, shutter controller, serial-to-ethernet converter, ethernet switch, etc. Armaflex insulation will be added to the CDC to prevent heat dissipation through the enclosure.

ACKNOWLEDGMENTS

This research was supported by the DFG cluster of excellence "Origin and Structure of the Universe". We wish to acknowledge the help and support of Spectral Instruments Tucson, Az. We also like to thank for the advice provided by the glueing experts of MPE Garching.

REFERENCES

[1] Hopp, U., Bender, R., Goessl, C., Mitsch, W., Barwig, H., Riffeser, A., Lang, F., Wilke, S., Ries, C., Grupp, F., and Relke, H., "Improving the Wendelstein Observatory for a 2m-class telescope," in [*Society of Photo-Optical Instrumentation Engineers (SPIE) Conference Series*], *Presented at the Society of Photo-Optical Instrumentation Engineers (SPIE) Conference* **7016** (July 2008).

[2] Hopp, U., Bender, R., Grupp, F., Barwig, H., Gössl, C., Lang-Bardl, F., Mitsch, W., Thiele, H., Aniol, P., Schmidt, M., Hartl, M., Kampf, D., and Schöggl, R., "The compact, low scattered-light 2m Wendelstein Fraunhofer Telescope," in [*Society of Photo-Optical Instrumentation Engineers (SPIE) Conference Series*], *Society of Photo-Optical Instrumentation Engineers (SPIE) Conference Series* **7733** (July 2010).

[3] Thiele, H., Ageorges, N., Kampf, D., Hartl, M., Egner, S., Aniol, P., Ruder, M., Hopp, U., Bender, R., Grupp, F., Barwig, H., Gössl, C., Lang-Bardl, F., and Mitsch, "New Fraunhofer Telescope Wendelstein: Assembly, Installation, and current Status," in [*Society of Photo-Optical Instrumentation Engineers (SPIE) Conference Series*], *Society of Photo-Optical Instrumentation Engineers (SPIE) Conference Series* **8444** (2012).

[4] Hopp, U., Bender, R., Grupp, F., Barwig, H., Gössl, C., Lang-Bardl, F., Mitsch, W., Thiele, H., Aniol, P., Schmidt, M., Hartl, M., Kampf, D., and Schöggl, R., "First Tests of the compact, low scattered-light 2m Wendelstein Fraunhofer Telescope," in [*Society of Photo-Optical Instrumentation Engineers (SPIE) Conference Series*], *Society of Photo-Optical Instrumentation Engineers (SPIE) Conference Series* **8444** (2012).

[5] Gössl, C., Bender, R., Grupp, F., Hopp, U., Lang-Bardl, F., Mitsch, W., Altmann, W., Ayres, A., Clark, S., Hartl, M., Kampf, D., Sims, G., Thiele, H., and Toerne, K., "A 64 Mpixel camera for the Wendelstein Fraunhofer Telescope Nasmyth wide-field port: WWFI," in [*Society of Photo-Optical Instrumentation Engineers (SPIE) Conference Series*], *Society of Photo-Optical Instrumentation Engineers (SPIE) Conference Series* **7735** (July 2010).

[6] Lang-Bardl, F., Hodapp, K., Jacobson, S., Bender, R., Gössl, C., Fabricius, M., Grupp, F., Hopp, U., and Mitsch, W., "3kk: the Optical-NIR Multi-Channel Nasmyth Imager for the Wendelstein Fraunhofer Telescope," in [*Society of Photo-Optical Instrumentation Engineers (SPIE) Conference Series*], *Society of Photo-Optical Instrumentation Engineers (SPIE) Conference Series* **7735** (July 2010).

[7] Fabricius, M. H., Barnes, S., Bender, R., Drory, N., Grupp, F., Hill, G. J., Hopp, U., and MacQueen, P. J., "VIRUS-W: an integral field unit spectrograph dedicated to the study of spiral galaxy bulges," in [*Society of Photo-Optical Instrumentation Engineers (SPIE) Conference Series*], *Presented at the Society of Photo-Optical Instrumentation Engineers (SPIE) Conference* **7014** (Aug. 2008).

[8] Fabricius, M. H., Grupp, F., Drory, N., Bender, R., Hopp, U., Arns, J., Barnes, S., Gössl, C., Hill, G. J., and Lang-Bardl, F., "VIRUS-W: commissioning and first-year results of a new integral field unit spectrograph dedicated to the study of spiral galaxy bulges," in [*Society of Photo-Optical Instrumentation Engineers (SPIE) Conference Series*], *Presented at the Society of Photo-Optical Instrumentation Engineers (SPIE) Conference* **8446** (2012).

[9] Pfeiffer, M. J., Frank, C., Baumueller, D., Fuhrmann, K., and Gehren, T., "FOCES - a fibre optics Cassegrain Echelle spectrograph," A&AS **130**, 381–393 (June 1998).

[10] Grupp, F., Udem, T., Holzwarth, R., Lang-Bardl, F., Hopp, U., Hu, S.-M., Brucalassi, A., Liang, W., and Bender, R., "Pressure and temperature stabilization of an existing Echelle spectrograph," in [*Society of Photo-Optical Instrumentation Engineers (SPIE) Conference Series*], *Society of Photo-Optical Instrumentation Engineers (SPIE) Conference Series* **7735** (July 2010).

[11] Grupp, F., Brucalassi, A., Lang, F., Hu, S. M., Holzwarth, R., Udem, T., Hopp, U., and Bender, R., "Pressure and temperature stabilization of an existing chelle spectrograph II," in [*Society of Photo-Optical Instrumentation Engineers (SPIE) Conference Series*], *Society of Photo-Optical Instrumentation Engineers (SPIE) Conference Series* **8151** (Sept. 2011).

[12] Grupp, F., Lang, F., Bender, R., Gössl, C., and Hopp, U., "A multi-instrument focal station for a 2m-class robotic telescope," in [*Society of Photo-Optical Instrumentation Engineers (SPIE) Conference Series*], *Presented at the Society of Photo-Optical Instrumentation Engineers (SPIE) Conference* **7014** (Aug. 2008).